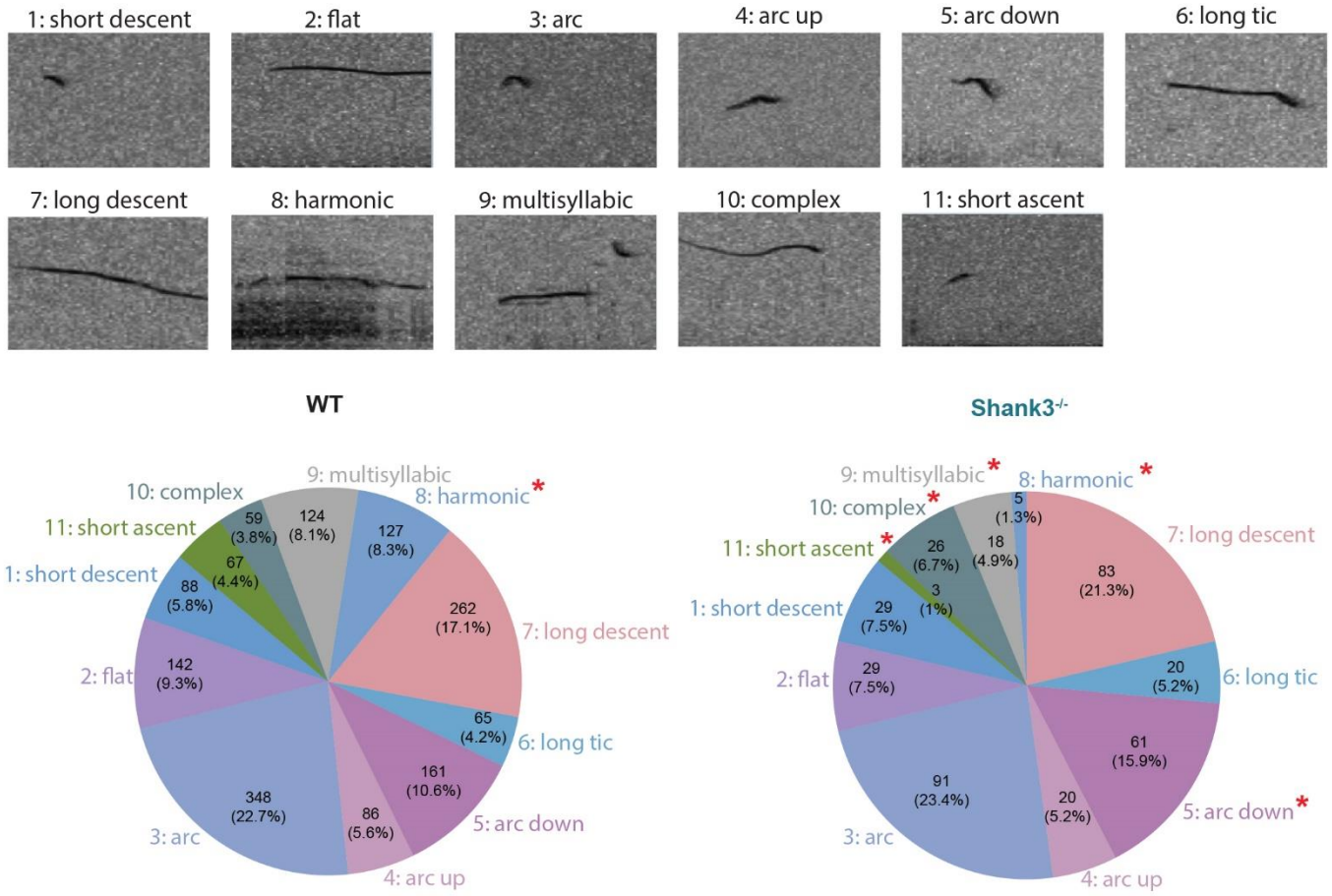

Supplementary Figure 1. P11 Shank3$^{-/-}$ mice exhibit altered ultrasonic vocalization (USV) category distribution. Top row: Examples of the main USV categories used for classification. Bottom: Pie charts showing the proportion of different USV categories for WT (left) and Shank3$^{-/-}$ (right) mice. A Chi-square test comparing the overall category distribution between genotypes is indicated at the bottom of the figure. Post hoc comparisons were performed using standardized residuals, and significant results ($p < 0.05$) are indicated with stars on the pie charts. A chi-square (χ^2) test was used to compare the overall distribution of USV types between genotypes. The chi-square test statistic was calculated as: $\chi^2 = \Sigma [(O_{ij} – E_{ij})^2 / E_{ij}]$ where O_{ij} is the observed frequency in cell i,j (e.g., genotype × USV category), and E_{ij} is the expected frequency for that cell under the null hypothesis of no association between genotype and USV category. Expected frequencies were calculated using the formula: $E_{ij} = (\text{row total})_i \times (\text{column total})_j / \text{grand total}$. To determine which specific USV categories contributed most to the observed group differences, a post hoc analysis was conducted using the standardized residual method. The standardized residual for each cell was computed as: Standardized Residual = $(O_{ij} – E_{ij}) / \sqrt{E_{ij}}$. Cells with large positive or negative standardized residuals indicate categories where the observed count is significantly higher or lower than expected. Significant deviations from expected frequencies are marked with asterisks to denote p-value thresholds.

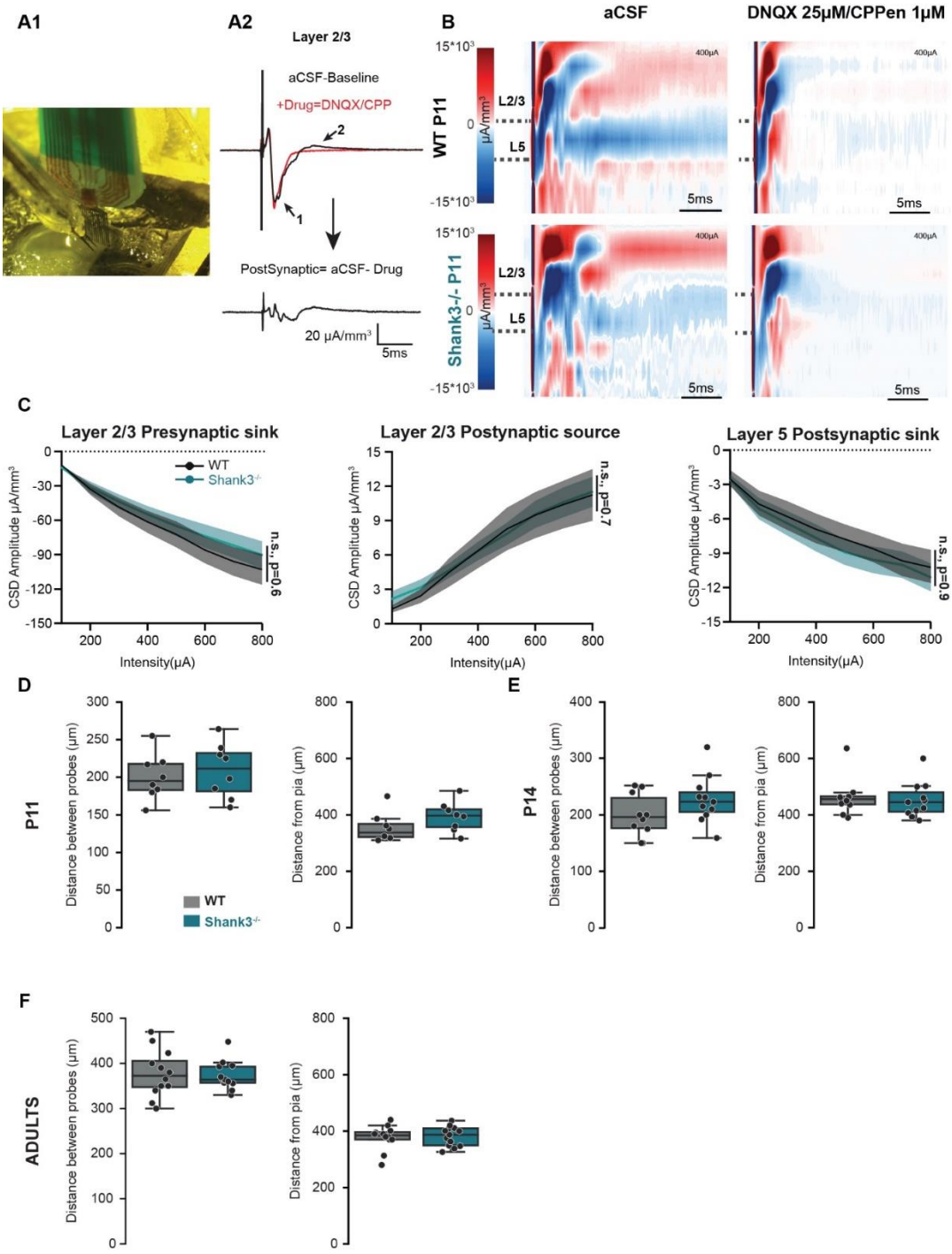

Supplementary Figure 2. mPFC slices from Shank3$^{-/-}$ mice display normal excitability at P11. (A1) Electrode placement for *in vitro* mPFC LFP recordings. (A2) Top panel: Representative CSD response recorded from the channel located in layer 2/3 under baseline conditions in ACSF (black). The trace exhibits two distinct components: a presynaptic component (indicated by arrow #1) and a postsynaptic component (indicated by arrow #2). Red trace: Following the application of DNQX (25 µM) and CPPENE (1 µM), only the presynaptic component (arrow #1) remains, as the postsynaptic component is blocked. Bottom panel: The subtraction of the drug-treated trace from the ACSF trace reveals the relatively smaller, isolated postsynaptic component. (B) Averaged CSD heatmap of mPFC network during 400 µA stimulation in P11 in WT (top) and Shank3$^{-/-}$ (bottom) littermates, before and after DNQX 25uM +CPPene 1uM bath application (8 slices in each case, from 2 animals). Postsynaptic responses are blocked by DNQX/CPPene, revealing the short-duration pre-synaptic component that is essentially complete within 5ms of the stimulus. This presumably reflects action potential firing

in presynaptic axons, as it was completely blocked by the sodium channel antagonist tetrodotoxin (not shown, n=3). Accordingly, responses blocked by DNQX/CPPene are postsynaptic, and mainly occur later than 5ms from stimulus onset. (C) Input/Output relationships for CSD peak amplitude across stimulus intensities ranging between 100 µA and 800 µA. Traces represent the mean (solid line) ± sem (shaded line) across multiple slices (n=8 slices, from 2 mice), and components 1, 2 and 3 are defined as in Figure 2. (D, E, F). Stimulation and recording electrode positions were equivalent for each genotype and at each developmental state: P11, P14 and adult, respectively. The distance between probes, i.e. the lateral distance between the stimulating electrode and the Neuronexus probe is shown on the left and the axial distance between the stimulating electrode and the pia is shown on the right. WT are in grey, Shank3$^{-/-}$ in blue.

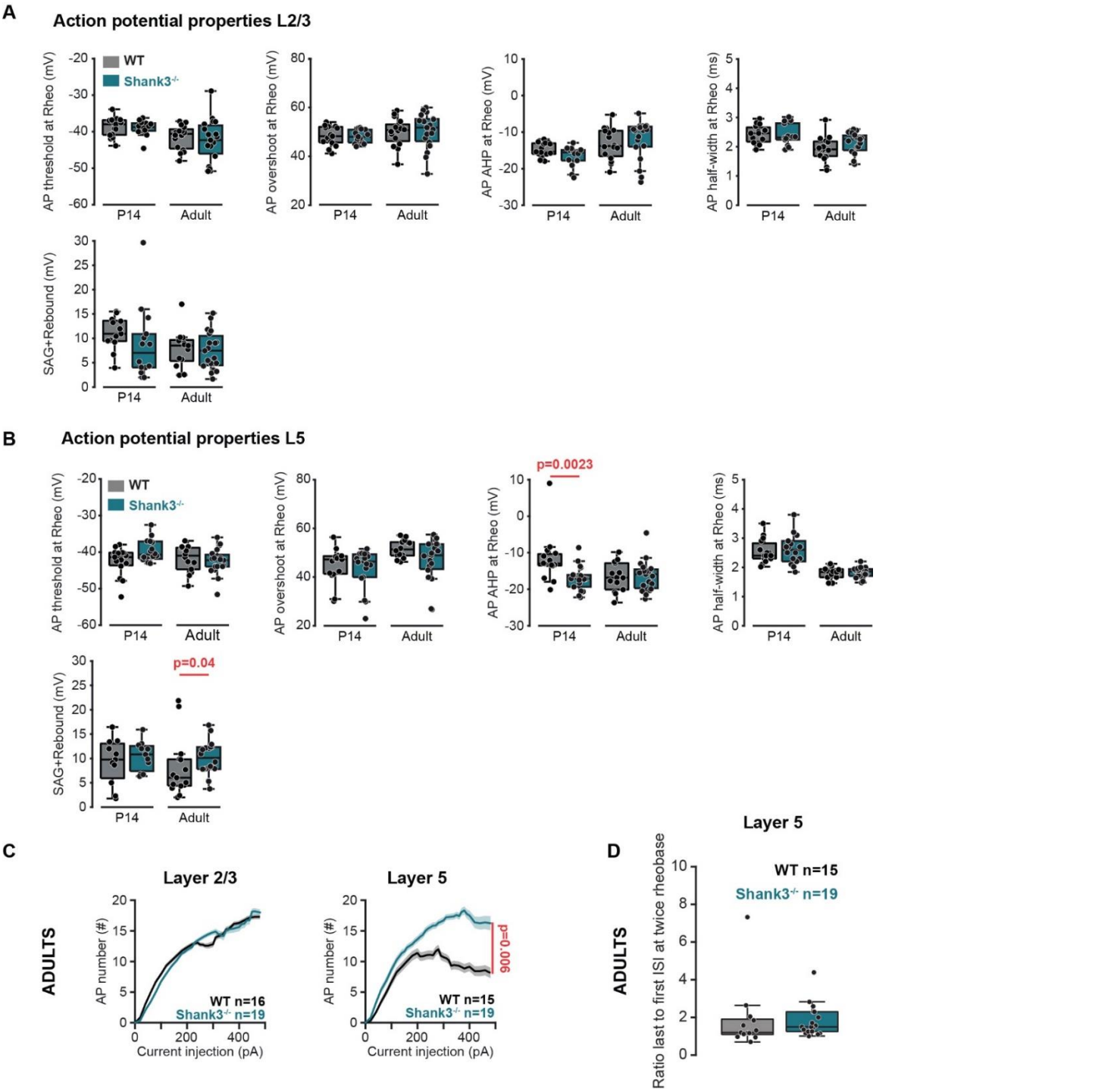

Supplementary Figure *3*. Layer 2/3 and layer 5 mPFC pyramidal cell action potential properties are largely unaffected in Shank3$^{-/-}$ mice, both at P14 and in adulthood. (A) Quantification of mPFC layer 5 pyramidal cells rheobase (rheo) action potential properties (threshold, overshoot, afterhyperpolarization (AHP), half-width) and sag+rebound, at P14 and adults for WT (grey) and Shank3$^{-/-}$ (blue). Sag+rebound is a composite measure of hyperpolarization-induced membrane potential sag and overshoot (see methods). (B) Quantification of mPFC layer 5 pyramidal cells rheobase action potential properties at P14 and adults for WT (grey) and Shank3$^{-/-}$ (blue). L5 cells show differences in only two properties, action potential afterhyperpolarization, and sag+rebound. (C) Action potential number across current injections in adult layer 2/3 (left) and layer 5 (right) pyramidal cells, including all recorded cells. Note the depolarization block observed in WT layer 5 cells. (D) Ratio of the first to last inter-spike interval at twice the rheobase for WT (grey) and Shank3^{-}/$^{-}$ (blue) layer 5 pyramidal cells.

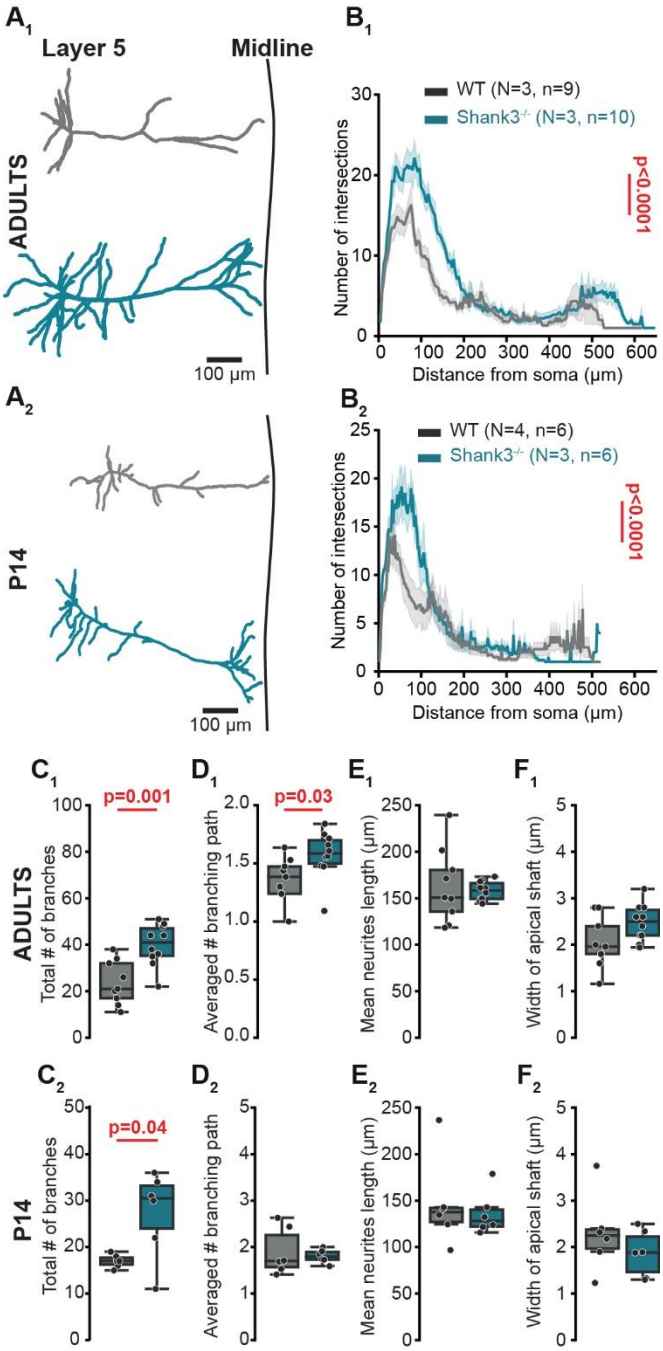

Supplementary Figure 4. mPFC layer 5 pyramidal neurons display increased dendritic complexity in Shank3$^{-/-}$ mice both in early life and in adulthood. (A) Representative examples of mPFC layer 5 pyramidal cells of adults (A1) and P14 (A2) WT (grey) and Shank3$^{-/-}$ (blue) mice reconstructed using biocytin reaction product, after filling during patch-clamp. (B) Average Scholl analysis of mPFC layer 5 pyramidal cells of adults (B1) and P14 (B2) WT (grey) and Shank3$^{-/-}$ (blue) adult mice. Traces are represented as mean ± sem. (C-F) Quantification of pyramidal cell morphological parameters (total number of branches, averaged number of branches, mean neurites length and width of the apical dendritic shaft) in adults (1) and P14 (2). WT are in grey, Shank3$^{-/-}$ in blue. (N is number of mice, n is the number of cells).

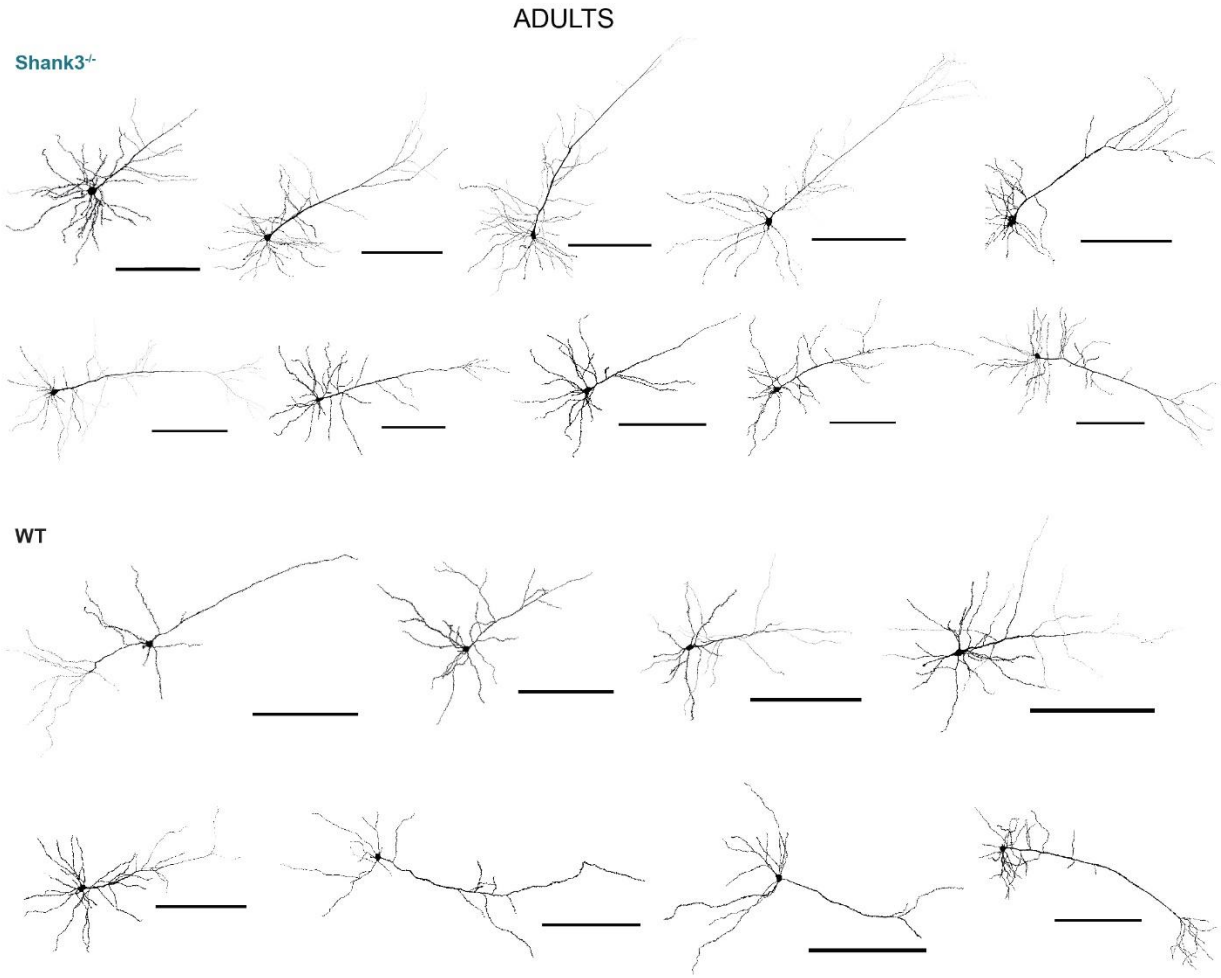

Supplementary Figure 5. Adult mPFC layer 5 pyramidal neurons filled with biocytin and reconstructed using the ImageJ SNT plugin. (A) Shank3$^{-/-}$ cells, showing more complex dendritic trees than (B) WT cells. Scale bar: 200 µm.

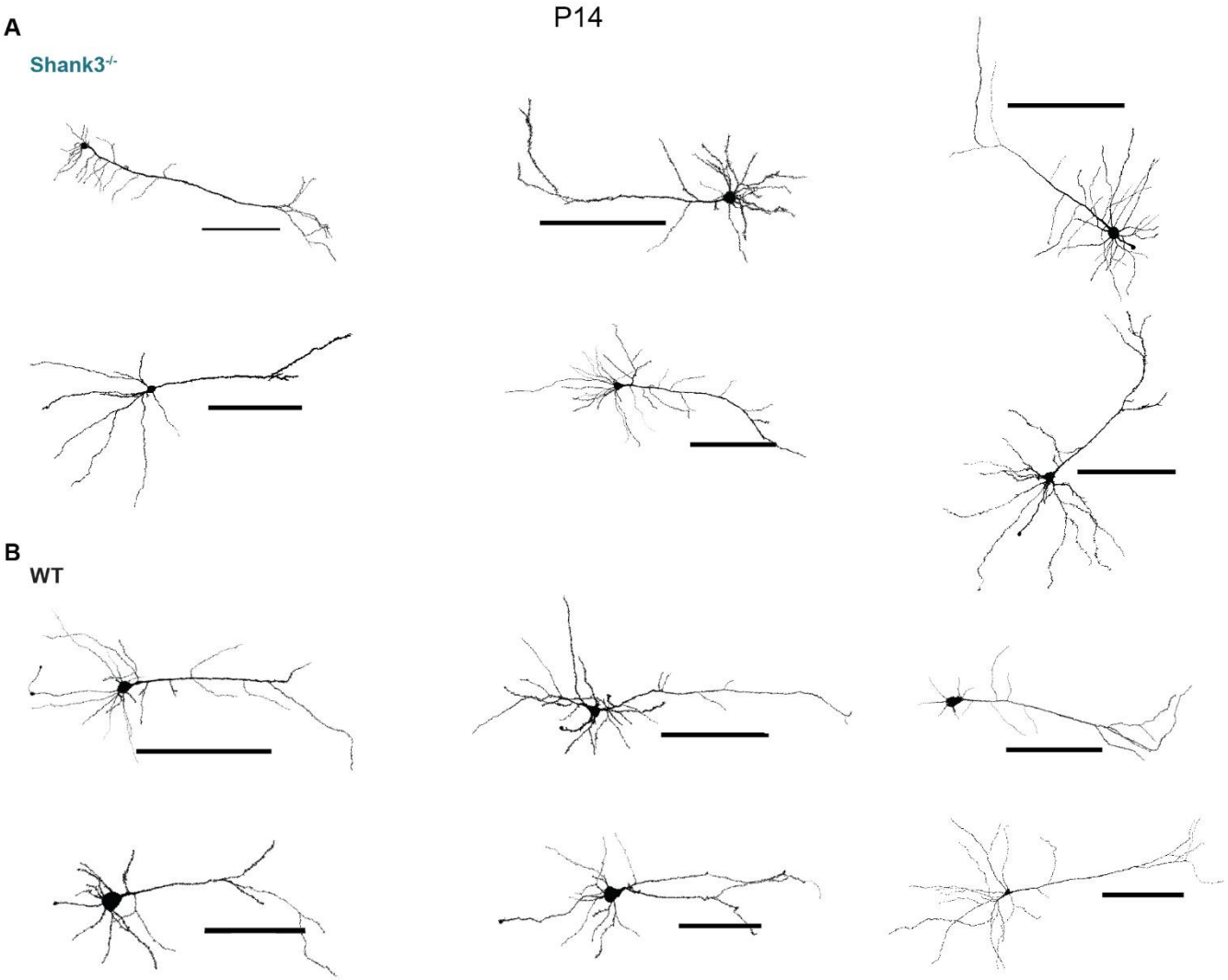

Supplementary Figure 6. P14 mPFC layer 5 pyramidal neurons filled with biocytin and reconstructed using the ImageJ SNT plugin. (A) Shank3$^{-/-}$ cells. (B) WT cells. Scale bar: 200 µm.

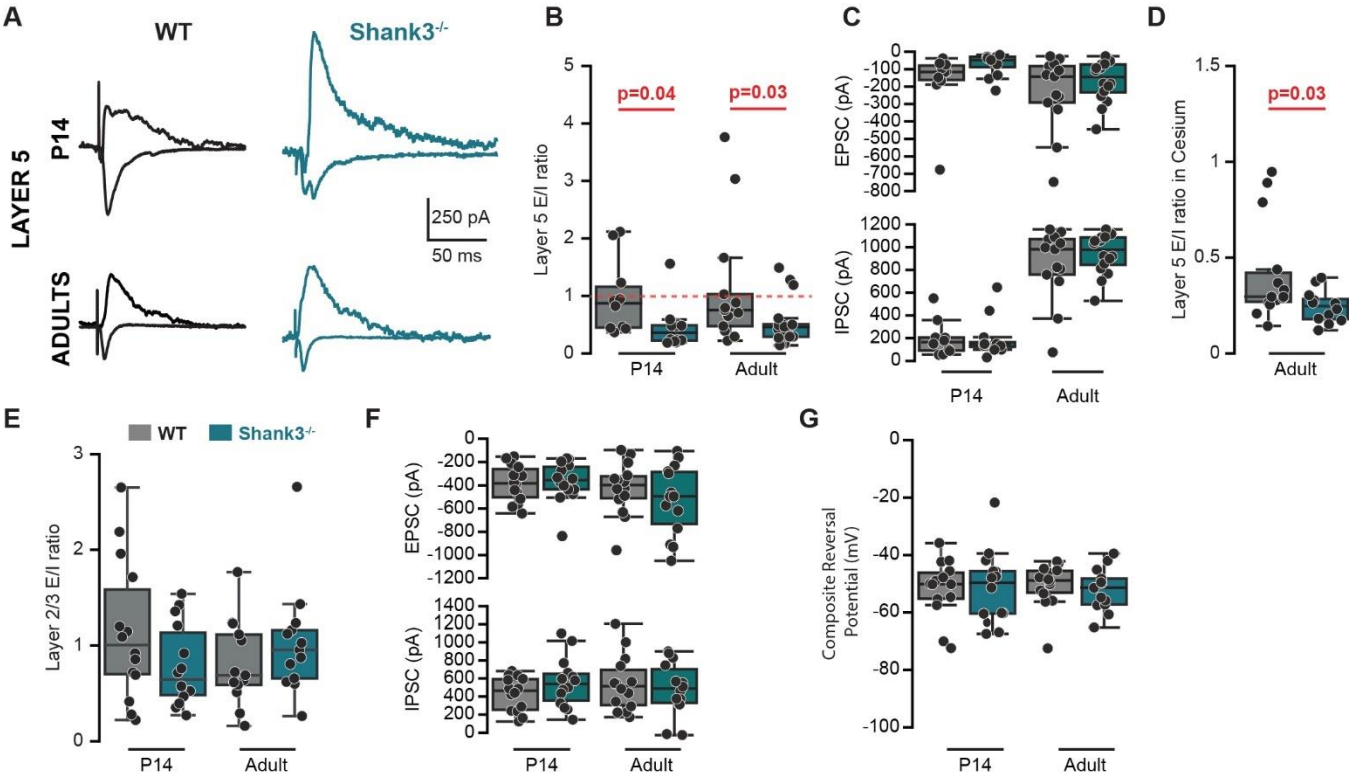

Supplementary Figure 7. Alterations in excitatory-inhibitory ratio in mPFC layer 5 pyramidal cells but not in layer 2/3 pyramidal cells of Shank3$^{-/-}$ mice. (A) Example traces of synaptic currents recorded from WT (gray) and Shank3$^{-/-}$ (blue) layer 5 mPFC neurons. Representative EPSCs were recorded at –70 mV and IPSCs at –30 mV. Traces from P14 mice are shown at the top, and traces from adult mice are shown at the bottom. (B) Ratio of excitatory to inhibitory synaptic currents (E/I ratio) recorded in layer 5 mPFC neurons from WT (gray) and Shank3$^{-/-}$ (blue) mice. (C) Box plots summarizing EPSC amplitudes (top) and IPSC amplitudes (bottom) recorded at –70 mV and -30 mV, respectively. Data are shown for all cells from WT (gray) and Shank3$^{-/-}$ (blue) mice, separated by developmental stage (P14, left; adults, right). (D) E/I ratio of adults mPFC layer 5 pyramidal cells, as determined by the ratio of electrically evoked synaptic currents measured at -70 mV and +10 mV, with a cesium based intracellular solution. (E) E/I ratio of mPFC layer 2/3 pyramidal cells at P14 (left) and adults (right). WT are in grey, Shank3$^{-/-}$ in blue. (F) Box plots summarizing EPSC amplitudes (top) and IPSC amplitudes (bottom) recorded at –70 mV and -30 mV, respectively. Data are shown for all cells from WT (gray) and Shank3$^{-/-}$ (blue) mice, separated by developmental stage (P14, left; adults, right). (G) Composite synaptic reversal potential of layer 2/3 mPFC neurons from WT (gray) and Shank3$^{-/-}$ (blue) mice.

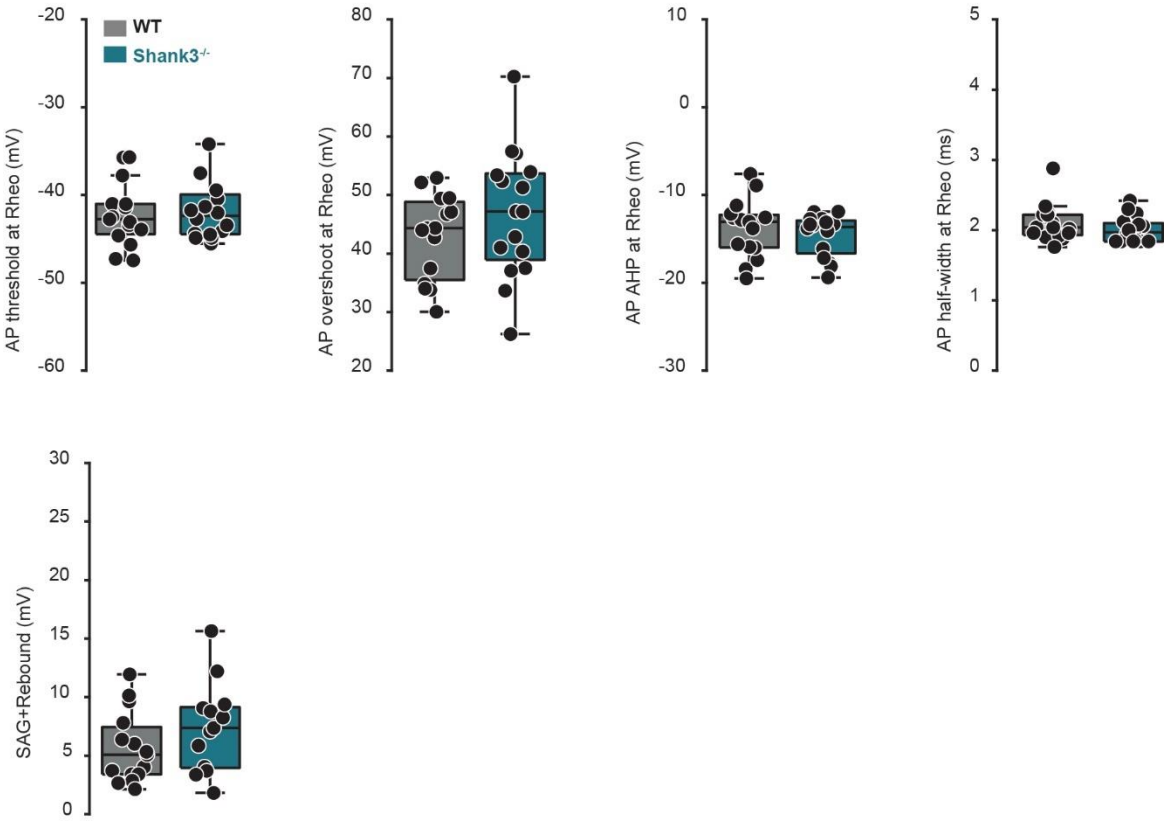

Supplementary Figure 8. Layer 5 mPFC pyramidal cell projecting to MD thalamus (PT cells) action potential properties are largely unaffected in Shank3$^{-/-}$ mice, both at P14 and in adulthood. Quantification of mPFC layer 5 pyramidal cells rheobase (rheo) action potential properties (threshold, overshoot, afterhyperpolarization (AHP), half-width) and sag+rebound, at P14 and adults for WT (grey) and Shank3$^{-/-}$ (blue). Sag+rebound is a composite measure of hyperpolarization-induced membrane potential sag and overshoot (see methods).

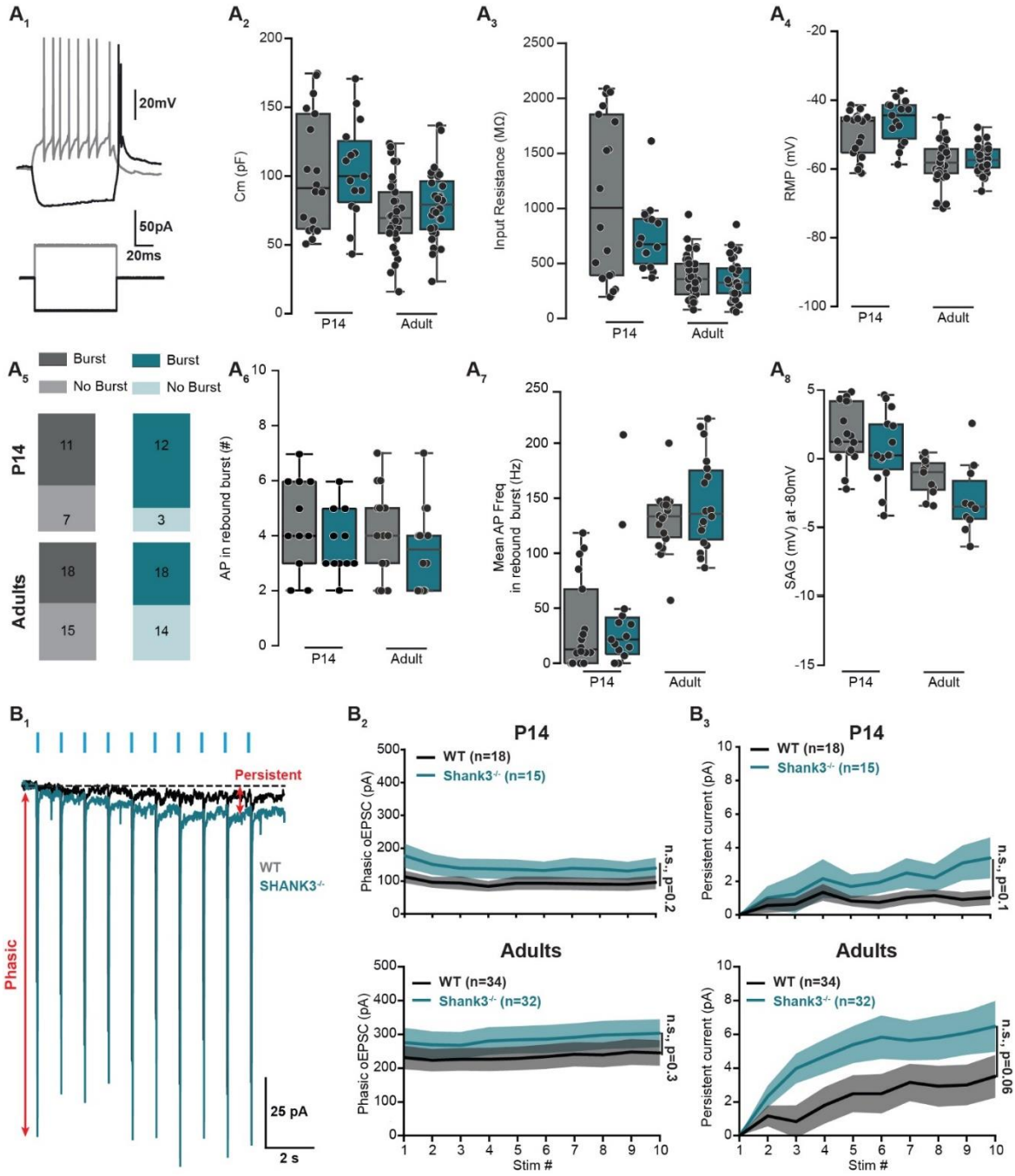

Supplementary Figure 9. Intrinsic electrical properties of MD neurons are unaffected by Shank3 knockout. mPFC-dependent excitatory synaptic responses show phasic and persistent components. (A) Example electrophysiological trace of an MD cell firing a rebound burst after a 50pA hyperpolarizing step (black) or tonic firing during a 50pA depolarizing step (grey) (1). Quantification of capacitance (Cm, 2), input resistance (3) and resting membrane potential (4) of adult MD cells of WT (in grey) and Shank3$^{-/-}$ (in blue). Characterization of the number of MD cells displaying a rebound burst (5), the number of action potentials within the burst (6), the mean action potential frequency within the burst (7), and the SAG measure when hyperpolarization reaches -80 mV in a subset of MD cells (8). (B) 1Hz optically evoked EPSCs (oEPCSs) show phasic and persistent responses, evident during stimulus trains. (B1) Representative oEPSC elicited with 1Hz stimulation in MD. Phasic and persistent measurement are indicated in red. (B2) Averaged phasic current quantification at

1Hz stimulation across 10 stimulations for adult WT (grey) and Shank3$^{-/-}$ (blue) mice. (B3) Averaged persistent current quantification at 1Hz stimulation across 10 stimulations for adult WT (grey) and Shank3$^{-/-}$ (blue) mice

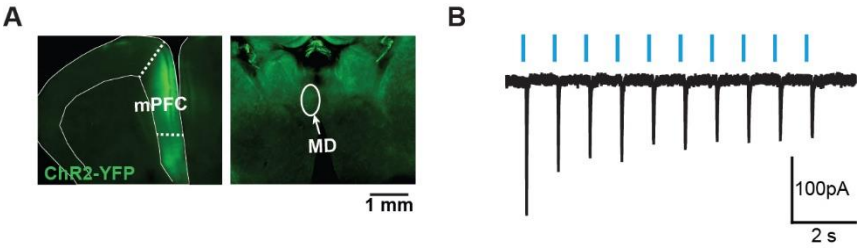

Supplementary Figure 10. Early postnatal mPFC injections result in functional optogenetic depolarizing responses responses axonal labeling in projections to MD. (A) left: A labeled image showing the injection site in the mPFC at P14 following injection at P0. Right: Axonal labeling visible in the mediodorsal thalamus (MD). (B) Optogenetically evoked responses recorded via patch clamp in a cell within the mPFC, indicating direct activation.

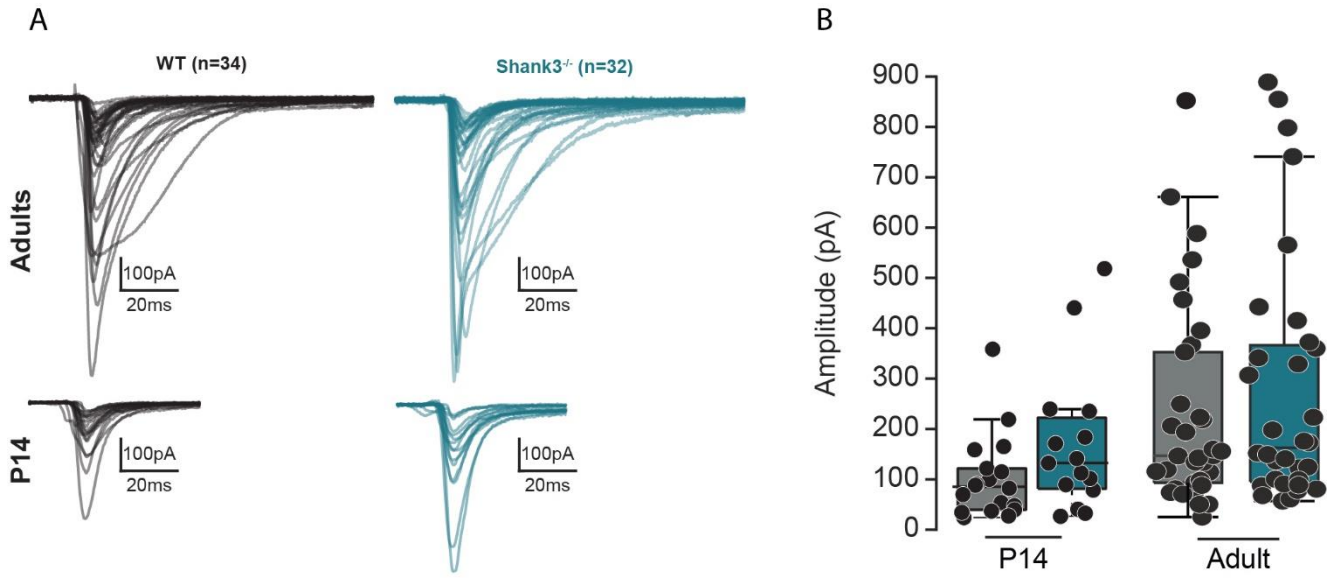

Supplementary Figure 11. Individual oEPSC amplitudes evoked in MD cells with 1 Hz stimulation in WT and Shank3$^{-/-}$ mice. (A) Individual traces of the first oEPSC evoked at 1 Hz stimulation for WT (black) and Shank3$^{-/-}$ (blue) cells in adult (top) and P14 (bottom) mice. **(B)** Boxplots showing the distribution of oEPSC amplitudes for each genotype and age group, with individual cell data points overlaid.

Table 1. Sex distribution for each experimental design using adult Shank3$^{-/-}$ and WT mice

FIGURE	TYPE OF EXPERIMENT	GENOTYPE	# MALE	# FEMALE	DRUG
1	Social Behavior	WT	4	2	NA
1	Social Behavior	Shank3	4	2	NA
2	LFP	WT	4	1	NA
2	LFP	Shank3	2	3	NA
3	PatchClamp mPFC	WT	4	2	NA
3	PatchClamp mPFC	Shank3	4	2	NA
3	EI ratio	WT	4	2	NA
3	EI ratio	Shank3	4	2	NA
4	Patch Clamp mPFC retrobeads	WT	3	0	NA
4	Patch Clamp mPFC retrobeads	Shank3	2	1	NA
5	PatchClamp Opto MD	WT	12	7	NA
5	PatchClamp Opto MD	Shank3	4	7	NA
6	PatchClamp Opto MD_drugs	WT	3	3	AP5
6	PatchClamp Opto MD_drugs	Shank3	0	3	AP5
6	PatchClamp Opto MD_drugs	WT	4	0	DHPG
6	PatchClamp Opto MD_drugs	Shank3	1	2	DHPG